




Joint European Research Infrastructure network for Coastal Observatory –
Novel European eXpertise for coastal observaTories - **JERICO-NEXT**

Deliverable title	Optimal OSE/OSSE infrastructure
Work Package Title	WP 3 Innovations in Technology and Methodology
Deliverable number	D3.11
Description	Report
Lead beneficiary	CMCC
Lead Authors	Guillaume Charria (IFREMER), Baptiste Mourre (SOCIB), Johannes Shultz (HZG), Eric Jansen (CMCC), Annalisa Griffa (CNR ISMAR) and Stefania Ciliberti (CMCC)
Contributors	
Submitted by	Stefania Ciliberti
Revision number	V1.1
Revision Date	31/10/2018
Security	Public





History			
Revision	Date	Modification	Author
V1.0		Not accepted due to open issues on CMCC activities (AMD-654410-31)	
V1.1	31/10/2018	Including CMCC activities (AMD-654410-31)	S. Ciliberti

Approvals				
	Name	Organisation	Date	Visa
Coordinator	Patrick Farcy	Ifremer	10/11/2018	PF
WP Leaders	George Petihakis	HCMR	01/11/2018	
WP Leaders	Laurent Delauney	IFREMER	01/11/2018	LD

PROPRIETARY RIGHTS STATEMENT

THIS DOCUMENT CONTAINS INFORMATION, WHICH IS PROPRIETARY TO THE **JERICO-NEXT** CONSORTIUM. NEITHER THIS DOCUMENT NOR THE INFORMATION CONTAINED HEREIN SHALL BE USED, DUPLICATED OR COMMUNICATED EXCEPT WITH THE PRIOR WRITTEN CONSENT OF THE **JERICO-NEXT** COORDINATOR.





Table of contents

1. Executive Summary	5
2. Introduction	6
3. Main report	7
3.1. The Bay of Biscay.....	7
3.1.1. Objectives and methodology.....	7
3.1.2. Ensemble numerical simulations.....	7
3.1.3. Ensemble and reference run validation.....	7
3.1.4. First results with HF Radar observing systems.....	9
3.1.5. Preliminary conclusions.....	10
3.2. The Ibiza Channel.....	11
3.3. The German Bight.....	13
3.3.1. Introduction.....	13
3.3.2. Calibration.....	14
3.3.3. Analysis using a combination of HF radar and tide gauge data.....	16
3.3.4. Conclusions and Outlook.....	16
3.4. The Central Mediterranean Sea: a focus in the Adriatic Sea and in the Ligurian Sea.....	18
3.4.1. Introduction.....	18
3.4.2. Description of the AIFS-EnKF DA modeling Framework and Validation.....	19
3.4.3. Description of the nature runs.....	19
3.4.4. OSE/OSSE infrastructure and experiments.....	19
3.4.5. Calibrated error statistics for OSSEs using OSSE/OSE results for the existing observation network in the W Adriatic and NW Med.....	20
3.4.6. Results of the transport analysis and verification in the NW Mediterranean and W Adriatic.....	22
3.4.7. Evaluation of transport in NW Mediterranean Sea.....	27
4. Outreach, dissemination and communication activities	28
5. Conclusions	28
6. Annexes and references	28







1. Executive Summary

This report concerns the results of Deliverable 3.11 “**Optimal OSE/OSSE infrastructure including biochemical transport**”, carried on in the task T3.7 “OSE/OSSE technology”.

It shows the main scientific results achieved by IFREMER, SOCIB, HZG, CMCC and CNR in defining a robust OSE/OSSE infrastructure for the future observing systems and modelling capabilities in the European Seas.

Results are organized by area and focus on the Bay of Biscay, the Ibiza Channel, the German Bight, the Adriatic Sea and the NW Mediterranean Sea.





2. Introduction

In T3.7, the new infrastructure for configuring optimal OSSEs has been developed using well-established standards (Halliwell et al., 2014) that require simulation and validation of a full-blown nature run and performing coupled OSE/OSSE for the existing observation network in each domain where OSSEs are performed. The nature runs for producing simulated observations are based on model simulations using a different forecast model or at least a significantly different version of the model than the one used in the data assimilation system, and will be verified using observations. The error statistics for each OSSE is calibrated based on the equivalent OSE, with both experiments performed for the existing observation network and the one developed within the JERICO-Next project. In this way, the assessments of value-added (i.e., the reduction of error) by potential new observations would be fully objective (the error would be measured relative to the quality of analysis with already available observations). This would ensure that the results produced in different regions and using different data assimilation systems will be compatible.

For the OSSEs in NW Mediterranean and Adriatic coastal regions (AIFS-DA), the nature runs have been produced using high-resolution modeling configuration based on Structured and Unstructured grid Relocatable ocean platform for Forecasting approach (SURF), developed by CMCC in collaboration with University of Bologna, that was especially designed for resolving the coastal ocean processes. HZG carried out fraternal-twin experiments in the German Bight where a reference model run has been perturbed by applying modifications to the wind forcing, the bathymetry, the bottom roughness, and the boundary forcing. Nature runs and calibration of the error statistics in the South-Eastern part of the Bay of Biscay (Ifremer/CNRS) has been done by using ensemble simulations based on coastal model configurations (sigma vertical layers, horizontal resolution around 1-2Km). Perturbations on the reference run will affect model parameters (e.g. turbulent-closure and light extinction coefficients), wind forcings, and initial conditions. Nature runs have been conducted in the Ibiza Channel by SOCIB and methodology here developed will be used to carry on the numerical experiments in JRAP#6.

The report is organized as follows: Section 3 presents the numerical experiments carried out in the Bay of Biscay, Ibiza Channel, German Bight, Western Adriatic and NW Mediterranean Sea; Section 4 will be devoted to conclusions.



3. Main report

3.1. The Bay of Biscay

3.1.1. Objectives and methodology

For the applications in the South-Eastern part of the Bay of Biscay, experiments are based on a method derived from data assimilation approaches based on a comparison between observed and modelled uncertainties. This recent method (Le Hénaff et al. 2009; Lamouroux et al., 2016; Charria et al., 2016), retained for this study and based on stochastic modelling, allows exploring a wide range of networks for different time periods. Based on a notion akin to the array modes as defined by Bennett (1985, 1990), the so-called ArM (Array Modes) methodology can be applied to evaluate the objective performance of a network design at detecting prior errors without having to run a fully assimilated system (as in usual OSSEs).

In the present project, the ArM (Array Modes) method has been extended to consider HF Radar observations with a joint application (collaboration with JRAP4 in WP4) in the South-Eastern Bay of Biscay including two HF radars system in Spain and a third system in the Southwest French coast (Figure 1). The HF Radar system along the French coast will be deployed in the frame of the present project based on results of OSSEs-like experiments.

3.1.2. Ensemble numerical simulations

These experiments need first to define the uncertainty of the model. To estimate these uncertainties, an ensemble of 50 perturbed simulations with the MARS3D model (4km spatial resolution, Lazure and Dumas, 2008) generated as a combined response to the following sources of errors is considered (Lamouroux et al., 2016; Charria et al., 2016):

- Uncertainties in the atmospheric forcings, which have been modelled through a 50-member ensemble of Gaussian-perturbed atmospheric fields (pressure at Sea Level, 10m-wind, Surface Heat Fluxes, 2m-temperature) provided by ECMWF;
- Uncertainties in specific model parameters, namely the bottom friction coefficient, the turbulent-closure coefficient and the light-extinction coefficient, which were slightly perturbed following a Gaussian distribution. Those parameters were retained since they have been shown to have a significant impact on the model results, and are - at least - partly uncorrelated (Friedrichs, 2001; Huret et al., 2007).

The ensemble covers the period from 15th January 2008 to the 15th February 2008.

3.1.3. Ensemble and reference run validation

The ensemble simulation and the reference run have been validated through comparison with remotely sensed (Sea Surface Temperature) and *in situ* observations.

The reference run is validated using remotely sensed Sea Surface Temperature (SST) based on SEVIRI Sea Surface Temperature data (METEOSAT SST provided by OSI-SAF belong to EUMETSAT with ~2km spatial resolution). Figure 2 shows an example of validation for the subregion in the South-Eastern part of the Bay of Biscay. The Taylor diagram shows a moderate correlation (between 0.6 and 0.7) and a relative standard deviation large than 1 representing a larger standard deviation in observations. These statistics confirm that the realism of the modelled SST can be improved. These gaps between modelled and observed dynamics can be explained considering two points. First, in this subregion, short upwellings appear with favourable winds for short periods. This upwelling dynamics is not fully reproduced by the model. The second point is related to the coarse resolution (4km) to reproduce dynamical processes in the region.

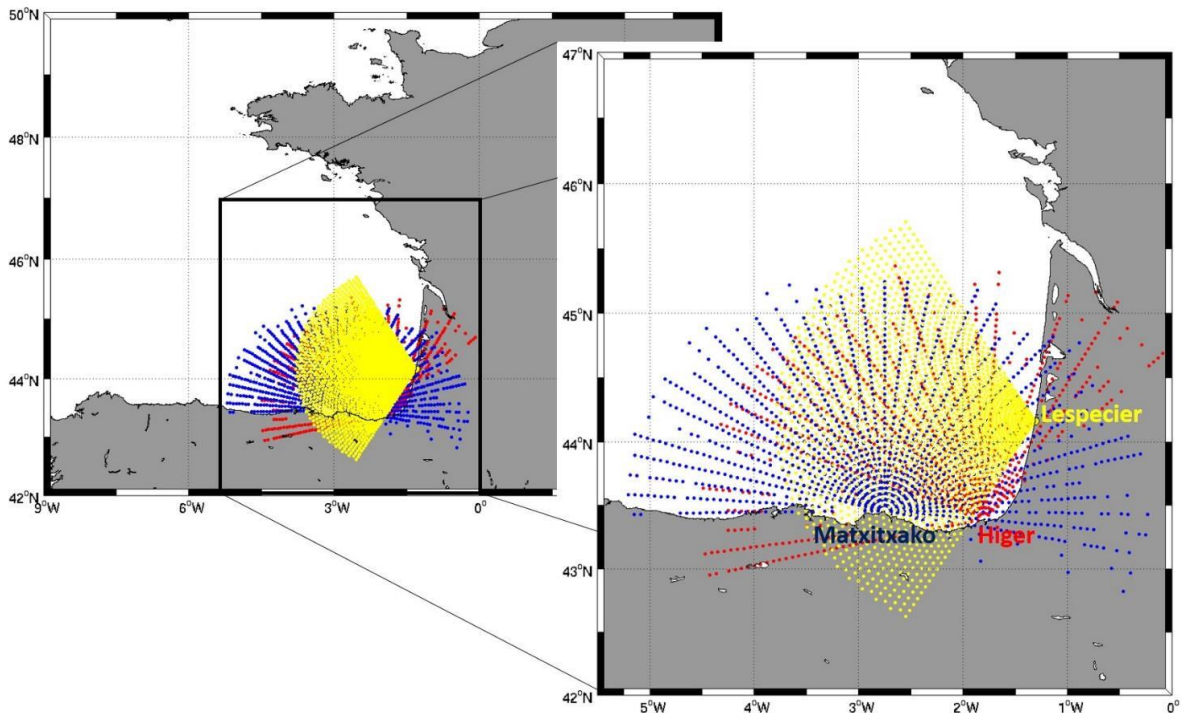


Figure 1: Illustration of three HF radar systems in the South-Eastern part of the Bay of Biscay including two existing systems (Matxitxako and Higer) and a future system deployed during JERICO-NEXT in 2017 (called "Lespecier").

Figure 3 gives an overview of the ensemble spread for the considered region. This spread remains limited (0.2-0.3°C) due to the model stability even in the case of larger parameter perturbations. Then, we observe that remotely sensed observations (Figure 3, right) are sometimes out of the ensemble spread.

In Figure 4, the ensemble standard deviation highlights the contrasted dynamics over the continental shelf, with larger standard deviation and the abyssal plain with smaller variability. Two river plume regions (Gironde around 45.5°N and Adour around 43.6°N) also appears as regions with a larger ensemble standard deviation on both velocity components.

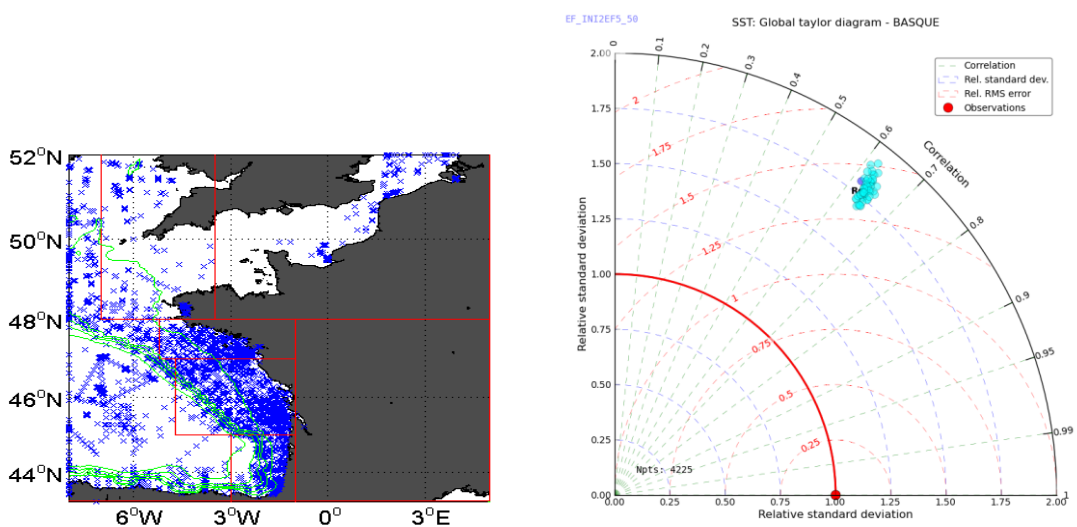


Figure 2: Map of subregions considered for validation (left) with a subregion centered on the South-Eastern Bay of Biscay named "BASQUE" (blue crosses represent position of available in situ profiles; green lines are isobaths). Taylor diagram (right) computed for this region comparing remotely sensed SST with reference simulation.

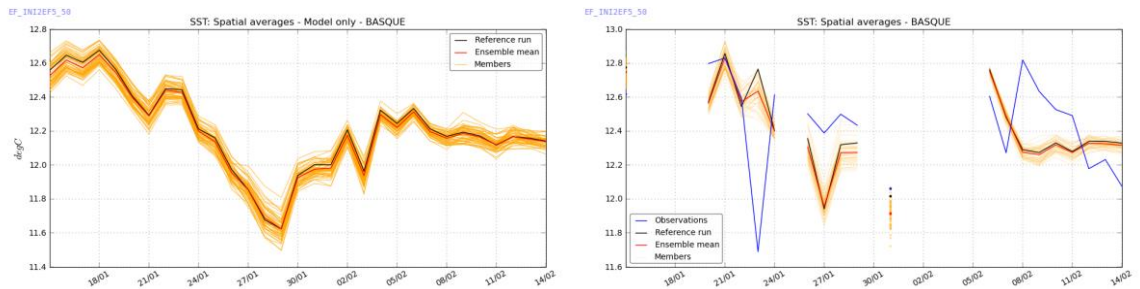


Figure 3: Time evolution of the ensemble spread (left) and subsampled for comparison with remotely sensed observations (right).

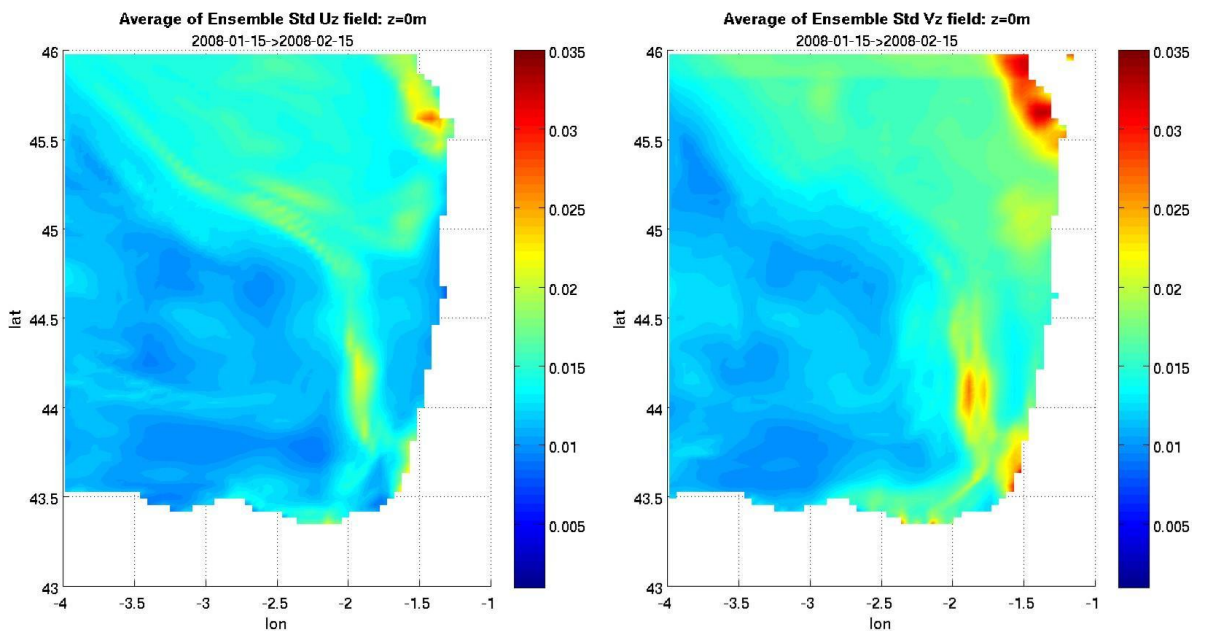


Figure 4: Temporal average of ensemble standard deviation from 15th January to 15th February 2008 in $m s^{-1}$.

Based on this ensemble and on existing properties of HF Radar operated by AZTI in Spain, a first version of the extended ArM method has been provided by the Noveltis company end of February 2016. First experiments based on the updated ArM methodology and the MARS3D ensemble have been performed. In a second step, an improved ensemble will be considered as a source of model uncertainties.

3.1.4. First results with HF Radar observing systems

In the present study, we explore the improvements of a third HF radar system along the French coast (deployed in WP4) supplying existing systems North of Spain: Higer and Matxitxako stations (Figure 1).

In this study, the Higer HF Radar is considered as the "reference network" (REF). The group of Higer and Matxitxako HF Radars represents the "network 1" (N1). The "network 2" (N2) is including both Spanish HF Radars and the third system on the French coast.

Higer and Matxitxako stations are using a 4.86 MHz frequency inducing a 200 km coverage from coast with 5 km radial sampling and an angular resolution of 5°. The third HF Radar system is located on the Landes coast (44°09.52'38"N, 1018.23'73"W). For the simulated system, the maximum distance of measurements is 200 km from coast with a spatial sampling every 1.5 km every 2° from -60° to +60°.

For the experiment, hourly fields are considered.

To use the ArM method, we need to define the observation error. In the present experiment, the observation error is $0.05 m s^{-1}$ for both U and V current components.

For each network, several diagnostics are considered:



- the eigenvalue spectrum of representer matrix to estimate the number of error modes detected by the network. This adimensional spectrum gives an estimation of the observing network efficiency.
- the modal representers associated with error modes detected by the network (not shown in this document).

Considering an observation error equal to 0.05 m s^{-1} , the Representer Matrix Spectrum (Figure 5) shows that both networks (N1 and N2) catches the errors modes solved in our simulations with 49 eigenvalue larger than 1. In the case of this network, the limited size of our experiment (50 members) does not allow distinguishing both networks. However, we can notice that the explained variance by first modes is more important in the case of N2 system related to the improvement due to the third HF Radar antenna along the French coast. Furthermore, this diagnostics clearly shows the importance of at least two HF Radar systems as a single antenna network clearly constrains less degrees of freedom of the system.

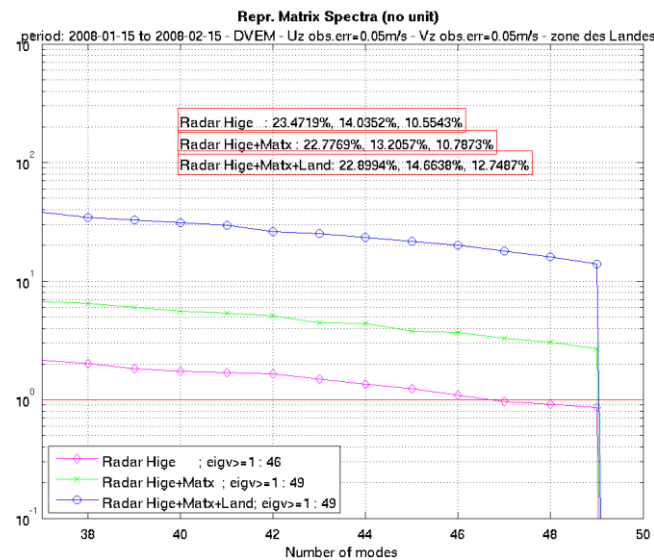


Figure 5: Representer Matrix Spectrum obtained for the three HF Radar networks for the period from 15th January to 15th February 2008.

A second preliminary experiment as been performed considering three potential positions of the HF Radar along the French coast (Figure 6).

From these three locations, three networks, including Spanish HF Radars have been tested. In the Representer Matrix Spectrum (Figure 7), networks are not distinguishable. This preliminary result leads to two main conclusions: the coverage for measurements is too similar for these three implementation sites and then similar dynamics is observed; the ensemble spatial resolution is too coarse to simulate the observed dynamics and then does not allow to discriminate these networks.

3.1.5. Preliminary conclusions

These first experiments show that the method has been successfully extended to HF Radar observation. However, the used ensemble with coarse spatial resolution (4 km) is not suitable to clearly evaluate the efficiency of the different networks.

Consequently, in the second phase of the projects, these experiments will be reproduced using ensemble with higher spatial resolution. Furthermore, during this first phase, possible improvements of the method (shape of observation operator) have been identified and will be implemented.

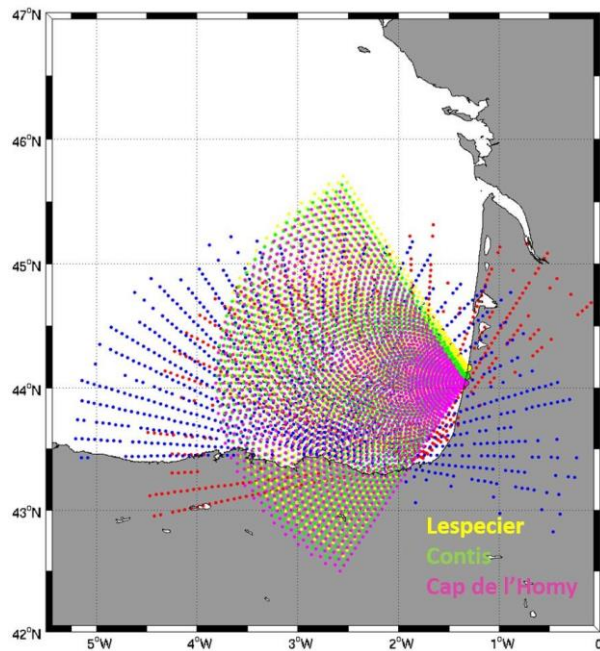


Figure 6: Three implementation sites along the French coast (Lespecier 44°09'52.38"N / 1°18'23.73"W, Contis 44°05'38,30"N / 1°19'29,45"W, Cap de l'Homy 44°02'20.49"N / 1°20'25.14"W).

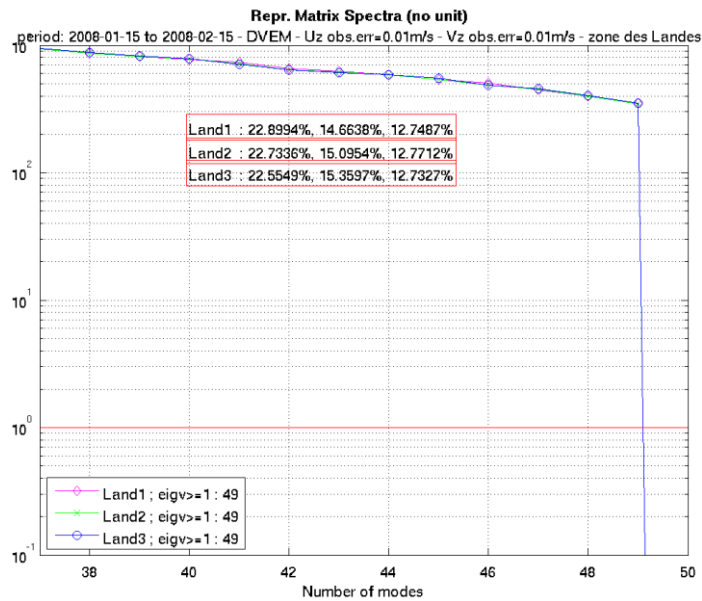


Figure 7: Representer Matrix Spectrum obtained for the three HF Radar networks (Land 1 = Lespecier, Land 2 = Contis, Land 3 = Cap de l'Homy) for the period from 15th January to 15th February 2008.

3.2. The Ibiza Channel

In the Western Mediterranean basin, the Balearic Sea constitutes a transition zone between the Liguro-Provençal sub-basin dominated by strong atmospheric fluxes, dense water formation events and a variable slope current, and the Algerian sub-basin marked by inflows of Atlantic water through the Strait of Gibraltar and an intense mesoscale activity. Moreover, the Balearic Islands exert strong topographic constraints on the circulation of water masses. In this context, the Ibiza Channel (70km wide and 800m deep approximately) represents a “choke point” for the north/south exchanges of the different water masses. It concentrates signals from different basin processes including surface circulation, mesoscale and intermediate water mass formation and propagation.



With two antennas located in Ibiza and Formentera Islands, SOCIB HF radar monitors the eastern part of the Ibiza Channel (Figure 8). The range of the instrument is presently insufficient to observe the western portion of the Channel where significant southward flows take place. In the framework of JERICO-NEXT JRAP#6, SOCIB will implement an Observing System Simulation Experiment aiming at evaluating the impact of a complementary HF radar installation along the Iberian Peninsula, then providing a full coverage of the Ibiza Channel. This experiment has been planned for the period M24-M40 of JERICO-NEXT project. The proposed approach and methodology is described here.

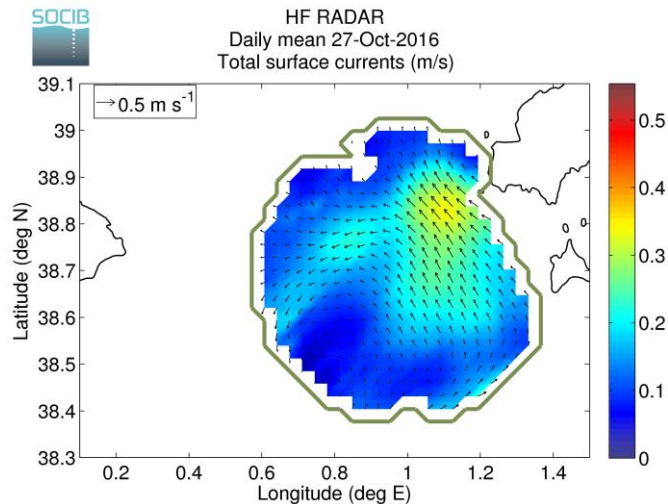


Figure 8. Present HF radar coverage and daily mean surface velocity measurements for 27 October 2016

The WMOP model (Juza et al., 2016) will be used to simulate the Western Mediterranean ocean dynamics. WMOP is a regional configuration of the ROMS model with a spatial resolution of 2km, using the CMEMS Mediterranean Forecasting System model as initial and boundary conditions.

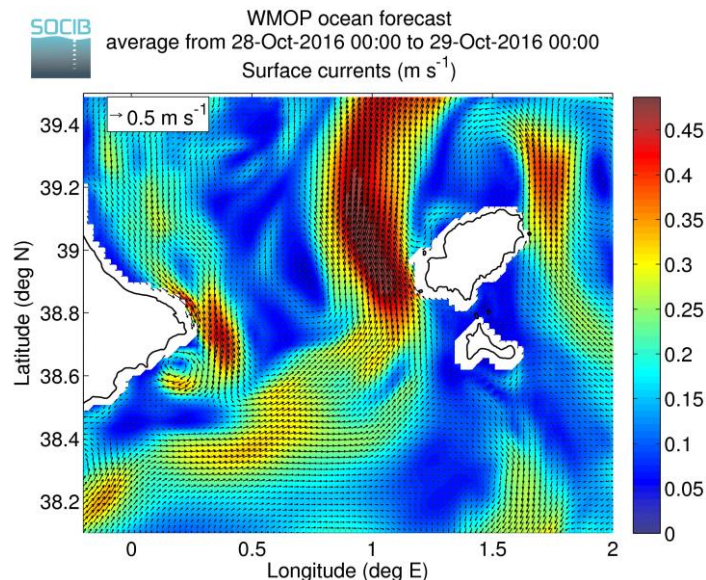


Figure 9. Example of operational WMOP velocity fields for 28 October 2016

The “nature run” will come for a reference WMOP hindcast simulation spanning the period 2009-2015 (Figure 9). This simulation will be especially validated in the Ibiza Channel for the purpose of the OSSE experiment. In particular, the dynamical modes of the model surface circulation will be compared to those deduced from the HF





radar measurements, both in terms of spatial and temporal scales. The downward looking ADCP mounted on SOCIB Ibiza Channel mooring will also be used to validate the vertical variability of model velocities in the upper 60m.

A perturbed simulation will be generated by modifying initial and boundary conditions as well as wind forcing with respect to the nature run. While a different large scale model will be used for initial and boundary conditions, the wind forcing will be perturbed based on a random recomposition of the signal using the main EOF modes.

HF radar velocities will be simulated from the nature run after addition of realistic measurement errors. A first OSSE will be computed over the actual radar coverage area to be able to perform an identical OSE (Observing System Experiment) assimilating the actual HF radar observations. OSSEs and OSEs should lead to compatible results to ensure that the simulation experiment system provides reliable estimates of the real impact of the observations (Halliwell et al., 2014). The study period will be determined according to the availability of HF radar data and independent validation measurements from the mooring and surface drifters. Two periods have been preselected in August and December 2014.

The final OSSE will then evaluate the impact of HF radar velocities in the western part of the Ibiza Channel using this validated OSSE system.

3.3. The German Bight

3.3.1. *Introduction*

The German Bight is a very shallow shelf sea area with maximum water depth of about 50 m. The dynamics is largely dominated by the semi-diurnal M2 tidal component with amplitudes of up to 1.5 m in the estuaries of the Elbe and Weser rivers. There are large Wadden Sea areas, which are actually falling dry during low tide. The bathymetry is quite complex and due to the small water depth it is a governing factor in the German Bight circulation. In the narrow channels leading into the Weser and Elbe river current speed can reach up to 1.5 m/s. Because of morphodynamic processes, the bathymetry can change on quite short time scales, in particular during storm events. Because of the costs and technical problems involved in measuring bathymetry there is quite a large error margin concerning bathymetric data.

The main challenges to be faced in numerical modelling of the German Bight circulation are as follows

- Uncertainties concerning bathymetry
- Uncertainties about bottom roughness
- Nonlinearities, e.g., due to wetting and drying
- Turbulence parameterisation

Because of the fact that the German Bight is a very busy area with an increasing number of user groups (e.g., shipping, fishery, offshore windfarming), it is also obvious that there is high demand for high quality information on oceanographic processes in the region. In this context there is growing interest in novel approaches for observations, numerical modelling and data assimilation.

The focus of HZG in the framework of the JERICO_NEXT project is on the investigation of HF radar surface current measurements in combination with traditional tide gauge data. HF radar measurements have been taken in the German Bight by three antenna stations located at the islands of Wangerooge, Sylt and on the mainland in Büsum for several years now. They have attracted quite some attention due to their potential to improve operational systems (e.g., for Search and rescue operations or for oil spill drift forecasts).

HZG has implemented a pre-operational assimilation system for the combination of HF radar measurements and numerical model data that is part of the COSYNA system. The respective analysis scheme was demonstrated to improve short term forecasts for surface currents with some upscaling capability (i.e., the surface currents can also be improved at locations outside the area covered by the radar) [Stanev et al., 2015].



It is clear that water level is an essential parameter for the coastal regions that should be estimated and predicted with high accuracy. Attempts to estimate water levels from HF radar data alone demonstrated that this is a challenging approach. The problem is that the water level dynamics is controlled by the divergence of the vertically integrated current field, i.e., in cases with more complicated vertical current profiles information on surface currents is not sufficient. A natural approach is then to combine the HF radar measurements with the traditional tide gauge observations, which are readily available at many locations.

The idea of the analysis of OSE/OSSE problems in the German Bight was to use a relatively simple model that is able to reproduce the main characteristic features of both currents and water levels, but at the same time allows easy tuning and inversion. The technical approach is similar to the method presented in Schulz-Stellenfleth and Stanev [2016]. The details of the implementation of the two layer model are described in Stellenfleth and Stanev [2017]. The main advantage of the method is that the model can be inverted. This is done in the spectral domain, which is a natural approach for the tidally dominated area anyway. The model contains parameters for bottom friction and for internal friction between layers. The prognostic variables are the zonal and meridional current components for the different layers as well as water level.

Figure 10 shows the M2 water levels amplitudes computed with the two-layer model (left) and the respective amplitudes derived from 16 tide gauges in the German Bight and two additional gauges at the Coast of Netherland and Denmark (right). One can see particularly high amplitudes of about 1.5 m around the Elbe estuary. The zonal surface current M2 component derived from the model (left) along with respective WERA Hf radar measurements are shown in Fig. 11. One can see current speeds of at least 1 m/s in the estuaries of the Weser and Elbe rivers.

The analysis is based on minimisation of the cost function

$$J(x) = (HMx - y)^H G^{-1} (HMx - y) + (x - \hat{x})^H P^{-1} (x - \hat{x})$$

where x is the control vector, G is the observation error covariance matrix, P is the prior error covariance matrix, M is the model operator, H is the observation operator, y is the measurements vector and \hat{x} is the first guess control vector. The subscript H denotes complex conjugation, because both the observations and the state vector represent complex spectral components. The control vector can contain various components – in this document we will concentrate on the case, where x represents the uncertain open boundary forcing. The operator M then translates this forcing into the respective current and water level fields.

3.3.2. Calibration

As explained in Halliwell et al. [2014] the different error models should be calibrated before OSSE experiments are performed. This applies to both the observation errors represented by the matrix G as well as the prior errors represented by the covariance matrix P . The basis of the analysis is a “nature run”, which should reproduce the main dynamical features of the system as good as possible. The nature run is used to simulate observations. In parallel we have a “fraternal Run”, which is either based on a completely different model or it is derived from the nature run by perturbation of different parameters. In the following presentation we will concentrate on perturbations of the open boundary forcing. Because of the ability to invert the two-layer spectral model we will take a slightly more general approach and look not only at one specific fraternal run but at the statistics that is used to generate fraternal runs. A natural requirement is that the departure of measurements simulated from the model by applying the observation operator H and subsequent addition of noise show a similar error characteristic as real measurements, i.e.

$$B^{real} \approx HMPM^T H^T + G$$

Where B^{real} is the covariance matrix of differences between real measurements and the numerical model.

As explained in Schulz-Stellenfleth and Stanev [2016] the standard deviation of water levels and currents can be readily computed from the used model if the covariance matrix of the perturbation is known. In a linear approximation the model equations can be written as

$$x = A^{-1}b,$$

where the vector x contains the state variables and the vector b contains boundary forcing and meteo forcing. If perturbations of the forcings are prescribed with covariance matrix C one has

$$xx^T = P = A^{-1}bb^T(A^{-1})^T = A^{-1}C(A^{-1})^T$$

for the covariance of the resulting state variables.

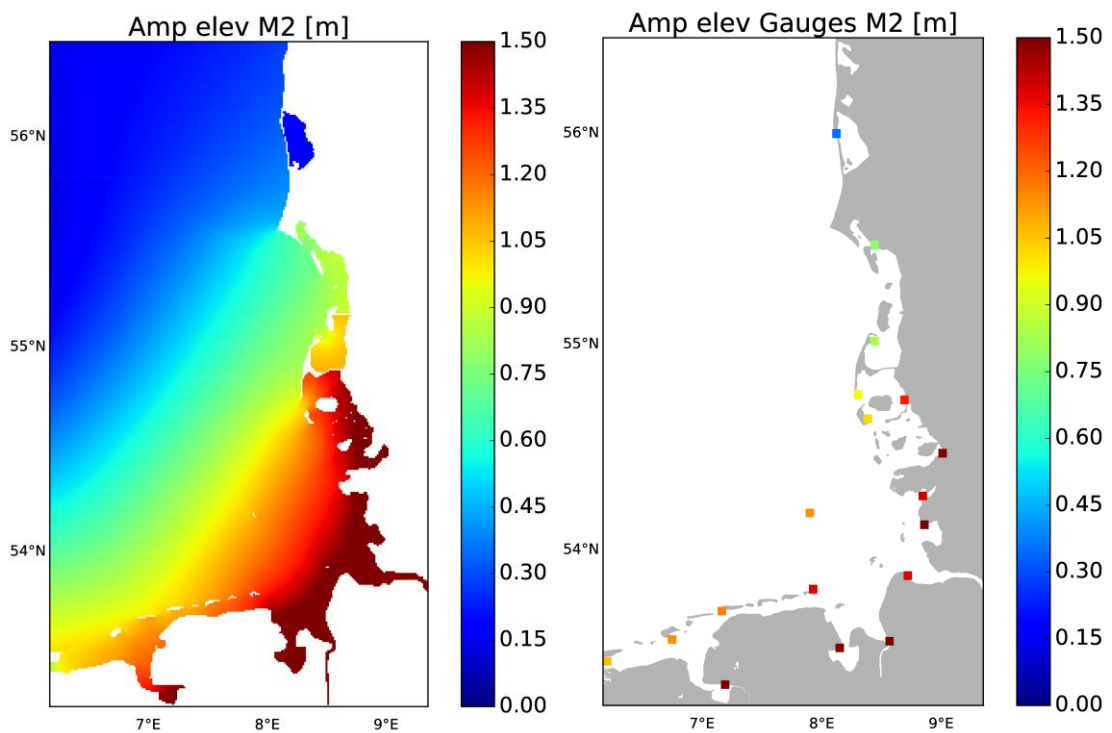


Figure 10. Comparison of M2 water level amplitudes computed with the two-layer model (left) and respective tide gauge measurements (right)

In Fig. 11 the results are shown for perturbations of the open boundary forcing with clamped conditions with standard deviation of 0.2 m and a correlation length of 30 km. The perturbations were chosen to approximately reproduce the deviations between model and real measurements at least in terms of order of magnitude.

As demonstrated in Schulz-Stellenfleth and Stanev (2016) this approach can be easily extended to perturbations of bathymetry and meteo forcing. In this case a Taylor expansion approach is applied, in which the forcing terms are expanded around the unperturbed solution.

As explained in Halliwell et al. (2014) it is in general not possible to find a perfect solution for the generation of fraternal runs, because the exact error sources of both the model and the observations are usually not known very well. However, what we have done here is to implement a calibration framework, in which first order consistencies of error models can be achieved and this is a major step forward.

3.3.3. Analysis using a combination of HF radar and tide gauge data

The error model described in the previous section was used to derive analysed water levels and current fields using different combinations of tide gauge and HF radar measurements. The analysis was computed by taking the gradient of the cost function

$$\nabla J(x) = 0$$

With the linearised model solutions can be found by solving a big complex valued linear system, which has a banded structure. As an efficient iterative technique a GMRES solver was used. As explained in Schulz-Stellenfleth and Stanev (2016) it necessary to compute the matrix S

$$S = HA^{-1}$$

where H is the observation operator. The matrix A^{-1} is quite big and cannot be stored in memory as a whole. The approach taken was therefore to compute columns of this matrix on the fly using a cluster computer. A linux cluster with MPI library was used for this purpose.

Different experiments were performed with the system using the following combinations of measurements

- EXP1** : Use both HF radar and tide gauge measurements
- EXP2** : Use only tide gauge measurements
- EXP3** : Use only HF radar measurements

Figure 12 shows the analysed water level amplitude as well as the surface current amplitude obtained by combined use of HF radar and tide gauge measurements. As one can see, by comparing to Figure 10 the amplitudes are slightly reduced in the river estuaries resulting in an improved agreement with measurements.

Table 1 shows the percentage reduction of the rms differences between model and observations for tide gauges and HF radar data separately. One can see that the use of the HF radar data or the tide gauge data alone is not sufficient to improve both water levels and currents at the same time. Only the combined use of both data sets leads to an improvement of both variables.

Experiment	Innovation – Residual water level [%]	Innovation - Residual Surface currents [%]
EXP1	25.9 %	11.4 %
EXP2	34.8 %	-1.6 %
EXP3	-2.4 %	16.2 %

Table 1: Innovations and residuals for different experiment with separation of tide gauge and HF radar contributions

3.3.4. Conclusions and Outlook

The analysis shows that there is a benefit in using a combination of tide gauge and HF radar measurements for transport estimations in the German Bight. The HF radar data provide valuable data for surface currents, but lack information on vertically integrated volume transports, which are connected to water level variations. By including water level measurements from tide gauges in the analysis this situation can be improved.

The presented method allows to analyse the contribution of current and water level measurements to transport estimations for different spectral components. By spectral decomposition of the wind field the impact of the meteo forcing can be included as well. The respective results will be used in JRAP4 to analyse volume transports through specific transects between the island of Helgoland to the mainland in east and south direction. In addition surface transports will be analysed with focus on drifting material (e.g., oil slicks)



We successfully implemented a technical framework to calibrate error models and to perform analysis with different types of measurements. As pointed out in Hallowell et al. [2014] this calibration will never be fully optimal due to the complexity of the different sources. The strength of the implemented tools is that they allow to further fine tune the models and analysis schemes in an iterative way as more information on modelling and observation errors become available.

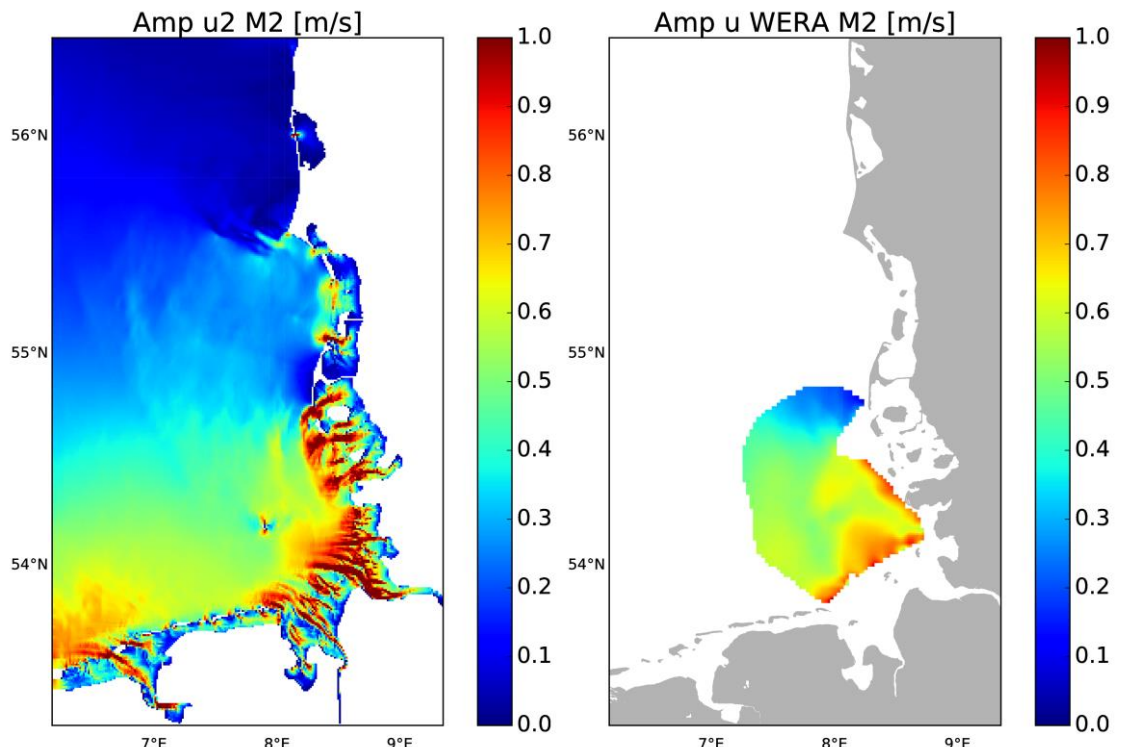


Figure 11. Zonal component of surface currents M2 amplitude estimated from two0later model (left) and corresponding estimated derived from HF radar (right)

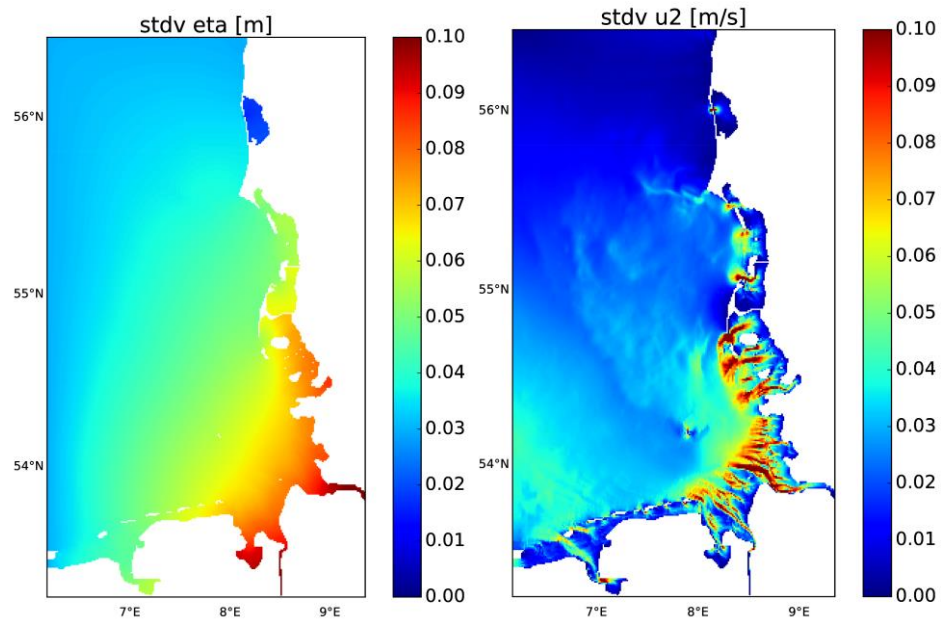


Figure 13. Standard deviation of water level resulting from open boundary forcing perturbations with 0.2 m standard deviation and 30 km correlation length (left). (right): The same for the zonal surface current component.

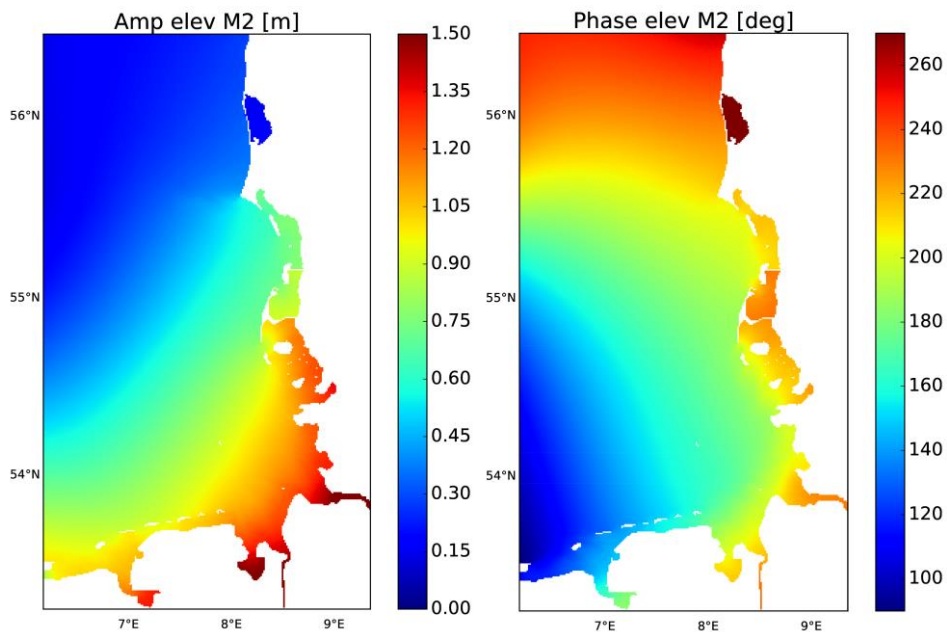


Figure 14. M2 amplitude (left) and phase (right) of analysis using both tide gauge and HF radar measurements.

3.4. The Central Mediterranean Sea: a focus in the Adriatic Sea and in the Ligurian Sea

3.4.1. Introduction

In order to test future instrument deployments and new observation types, an OSE/OSSE infrastructure was developed based on the AIFS model. Following the recommendations of Halliwell (2014), the AIFS-EnSRF assimilation system is paired with another NEMO-based model at very high resolution. This twin model uses



the SURF relocatable model (Trotta, 2016) at $1/64^\circ$ horizontal resolution to provide synthetic observations for the AIFS-EnSRF system.

3.4.2. Description of the AIFS-EnKF DA modeling Framework and Validation

The Adriatic-Ionian Forecasting System (AIFS) is a NEMO-based model for the central Mediterranean Sea. It uses a horizontal resolution of $1/45^\circ$ (approximately 2km) and 121 vertical levels. Data assimilation in this system is performed using a Python implementation of the Ensemble Square Root Filter (EnSRF) of Whitaker and Hamill (2002). The filter is coupled to the model in offline mode.

The ensemble for the EnSRF is generated from a 12-year historical run (2003-2014). Using the restart files of the nominal model, perturbations are added by sampling the daily average fields for 3 days from each year. These days are spaced 14 days apart and centered on the nominal date. The mean over all days is subtracted from the fields and replaced by the fields of the nominal model. Each day then becomes the perturbation for one ensemble member. The perturbed fields are temperature, salinity and the zonal and meridional velocities.

3.4.3. Description of the nature runs

The high resolution model setup used for organizing the OSSEs in the Adriatic Sea and in the NW Mediterranean is based on the Structured and Unstructured grid Relocatable ocean platform for Forecasting approach (SURT, Trotta et al., 2016). The activity has been carried on in collaboration with University of Bologna.

The module used within JERICO-Next is based on the structured grid hydrodynamic model based on NEMO ocean model (Madec et al., 2008). Conceptually, SURF is designed to work as a child model, one-way nested into a parent model at coarser resolution. The parent model used for providing initial and boundary conditions to high resolution setup in the Central Mediterranean area is the operational GOFS16 (Global Ocean Forecasting System) developed and maintained operational by CMCC (Iovino et al., 2016, 2018). Two model configurations have been developed in the Central Mediterranean area: one covering the Adriatic Sea, including the Northern Ionian Sea (over the bounding box $12.0^\circ\text{E} - 22.0^\circ\text{E}$; $36.0^\circ\text{N} - 46.0^\circ\text{N}$) and one covering the Ligurian Sea (over the bounding box $7.5^\circ\text{E} - 11.5^\circ\text{E}$; $42.0^\circ\text{N} - 45.0^\circ\text{N}$). The primitive equations are discretized on a horizontal grid at $1/64^\circ$ horizontal resolution and 100 vertical levels with partial steps, with first level model depth at 0.6 m, reaching a very high resolution in the vertical direction. A numerical experiment has been performed over 3-months period, from Jan 2017 to Mar 2017 and hourly means for 3D temperature and salinity at observation locations, described in the next subsections, have been considered to perform OSE/OSSE.

3.4.4. OSE/OSSE infrastructure and experiments

To validate the OSE/OSSE system, a validation experiment is performed over a 2-month period. During this experiment both an OSE and an OSSE are performed. For the OSE the observations are regular ARGO profiles of temperature and salinity for all ARGO profilers located in the Adriatic and Ligurian Seas during this period. The OSSE assimilates the same observations, but uses synthetic ARGO profiles. These synthetic ARGO profiles are extracted from the high-resolution nature run, at the same time and location of the regular ARGO profiles. Assimilating real profiles in the OSE and the corresponding synthetic profiles in the OSSE constitutes the twin-experiment setup that can be used to evaluate the differences between the OSE and OSSE.

A first visual evaluation can be performed by comparing the real and synthetic profiles to the model values. An example of this comparison is shown in Figure 12. In general the differences appear to be similar between the model and the two types of profile. The higher-resolution nature model performs better overall in modelling the ARGO profile than AIFS.



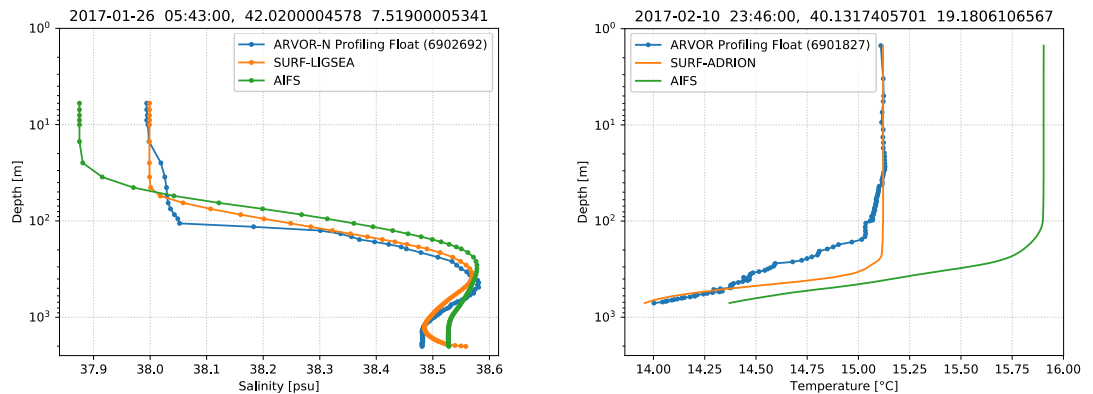


Figure 12: Examples of profiles from ARGO (blue), the nature run (orange) and the AIFS model without data assimilation (green). The left panel shows a profile in the Ligurian Sea, while the right shows a profile in the Adriatic Sea.

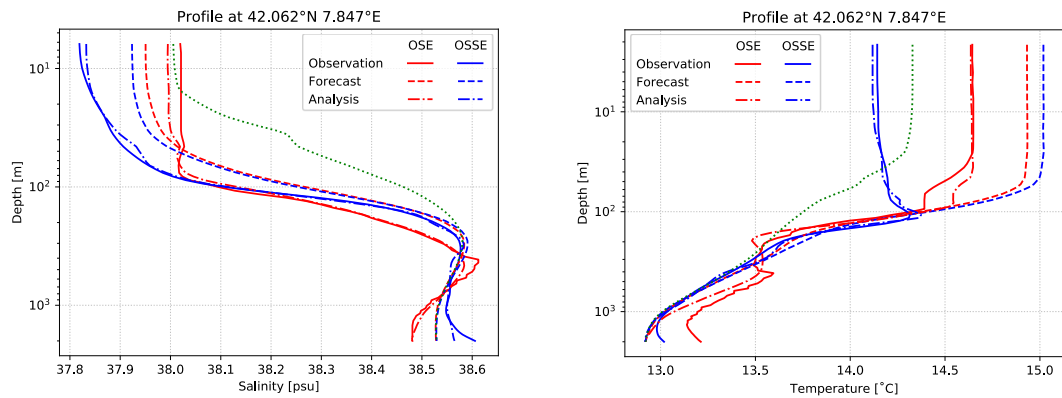


Figure 13: Example of the assimilation of a profile in the OSE (red) and OSSE (blue). The initial state is indicated by the dashed line, after assimilating the observation (solid line) the analysed is the dash-dotted line. The dashed green line shows the free run of AIFS for comparison.

When assimilating observations, corrections are applied to the ensemble. In the ensemble, the variations between the ensemble members are used to estimate of the model covariance. Therefore the impact of observations will vary based on prior information contained within the model, and the impact may vary even between the OSE and OSSE for the same time and location. An example of the assimilation of a temperature and salinity profile is shown in Figure 13.

3.4.5. Calibrated error statistics for OSSEs using OSSE/OSE results for the existing observation network in the W Adriatic and NW Med

Aggregated results for the full period are shown in Figure 14 and Figure 15. Differences found between the OSE and OSSE experiments are of the order of 10% or less. The only significant difference is observed for salinity near the surface, where the synthetic observations are further from the model than the real observations. Below approximately 3m depth also salinity shows good agreement between the OSE and OSSE.

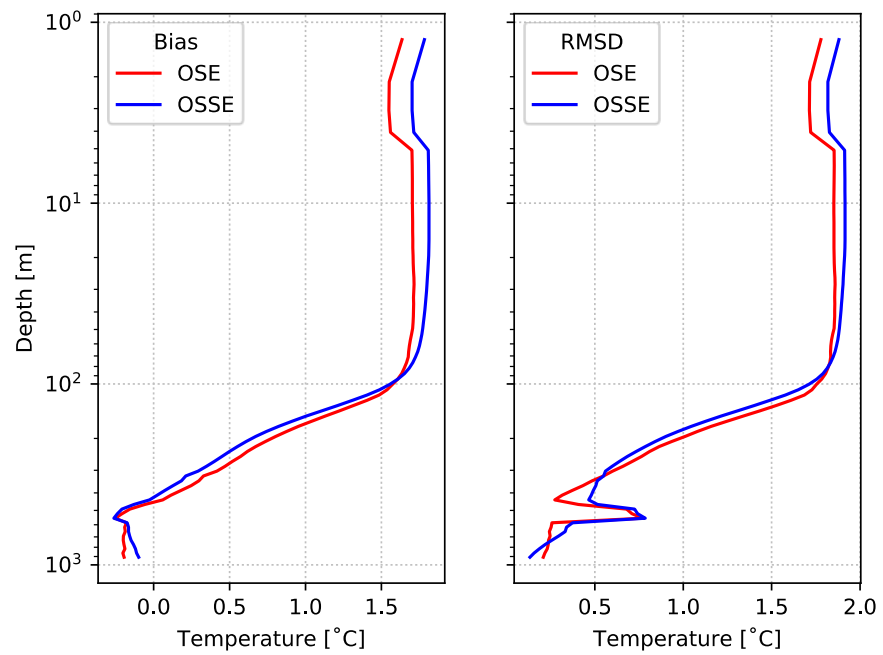


Figure 14: Bias and RMSD for temperature as a function of depth for the full period of the OSE/OSSE experiment. The OSE is shown in red while the OSSE is shown in blue. Both curves show good agreement, with differences of up to 10%.

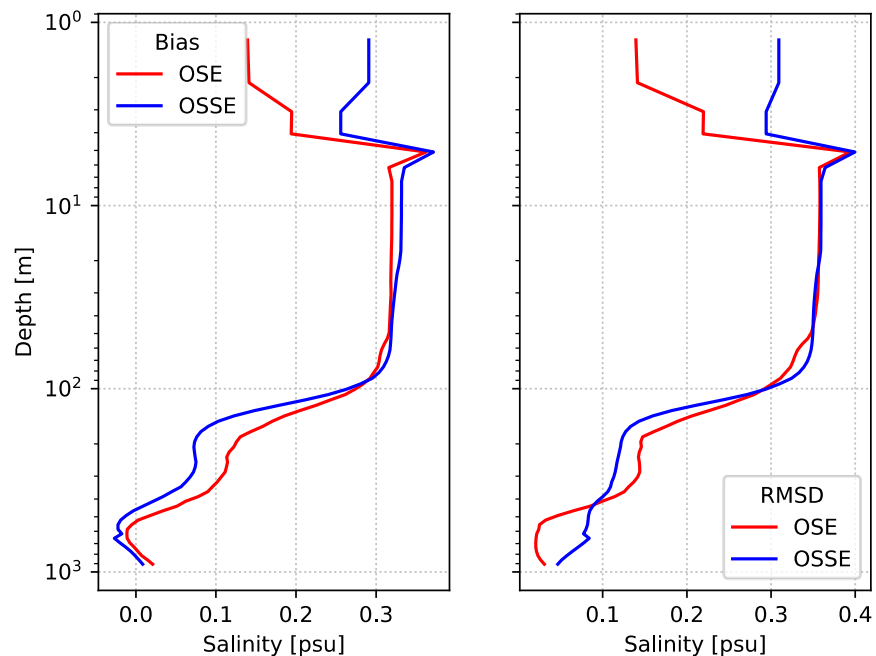


Figure 15: Bias and RMSD for salinity as a function of depth for the full period of the OSE/OSSE experiment. The OSE is shown in red while the OSSE is shown in blue. Both curves show good agreement over most of the depth range, except in the near-surface salinity where the nature run shows a larger bias than ARGO.

3.4.6. Results of the transport analysis and verification in the NW Mediterranean and W Adriatic

Observational Data

HF radar surface current velocity observations in the Adriatic Sea are provided by four antennas near the Gulf of Manfredonia in Italy, as shown in Figure 16. Two antennas inside the gulf (Manfredonia and Mattinata), while two others (Pugnochiuso and Vieste) are located on the cape. While the first two antennas provide a good stereo-angle and are therefore able to reconstruct u- and v-components of the surface currents, the two antennas on the cape measure mostly the u-component.

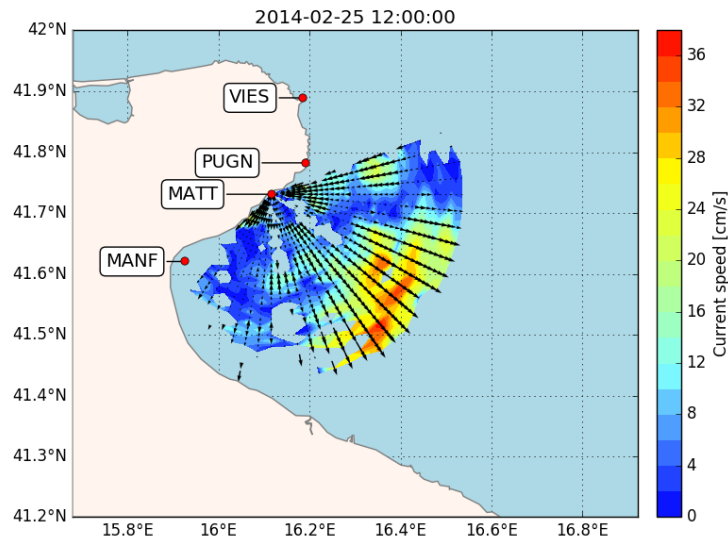


Figure 16: Location of the four HF radar antennas near the Gulf of Manfredonia. The typical range of an antenna is illustrated by superimposing the data measured by the antenna in Mattinata.

In addition to the radar data, drifter data were acquired from CNR to perform validation experiments. During the time window for the Observation System Experiment (OSE), 2014/02/26 - 2014/03/09, a total of five surface drifters were deployed within the radar coverage.

Procedure for assimilating HF radar observations

In order to make the best use of the available data, the assimilation system uses directly the radial velocity that is measured by the antenna, without reconstructing u or v from this data. While this is slightly more complicated on the side of the observation operator, the major benefits are that:

- All data can be used, including areas that are covered by only a single antenna;
- Uncertainties are correctly represented by the ensemble, as in general they will be much larger parallel to the coast.

Radar velocities are assimilated for each antenna separately. A preprocessing is performed in which the data of an antenna is averaged over the assimilation window and subsequently the density of the data is reduced to match the resolution of the model. The matching is done by assigning each observation to the closest location on the model grid, then for each grid point retaining only the closest observation. The other observations are dropped. This results in a radial velocity field with uniform density within the entire radar coverage. This is illustrated in Figure 17.

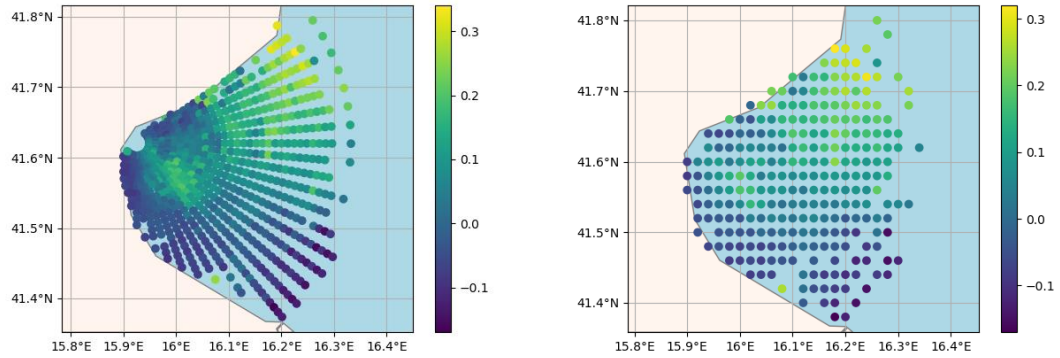


Figure 17: Gridding of the HF radar data. The raw data (left) is matched to the model grid and redundant data is removed to avoid overfitting in areas where the resolution of the observations is much higher than the resolution of the model. The colour scale indicates the scalar current velocity measured by the radar antenna.

Results and validation

Three experiments are performed with the system in order to evaluate its performance, their parameters are summarised in Table 2. All experiments take place in the same period and location, but the parameters of the assimilation vary. Experiments 1 and 2 assimilate HF radar data only at 12pm UTC, considering an assimilation window of 11:30am until 12:30pm. HF radar data outside this window is therefore not used. The observational uncertainty is assumed to be uncorrelated and fixed at 1cm/s for experiment 1 and 0.5 cm/s for experiment 2.

Table 2: Summary of the parameters for the three experiments.

Experiment	Observational uncertainty [cm/s]	Assimilation frequency
1	1	daily
2	0.5	daily
3	1	hourly

In Figure 18 the result of assimilating a typical radial observation into the ensemble is shown. The red distribution shows the distribution of the observation background predicted by the ensemble. The distribution is approximately Gaussian and covers a wide range of velocities. After using the Kalman filter to assimilate the observation (indicated by the line), the ensemble spread reduces to the green distribution and the mean value shifts towards the observation.



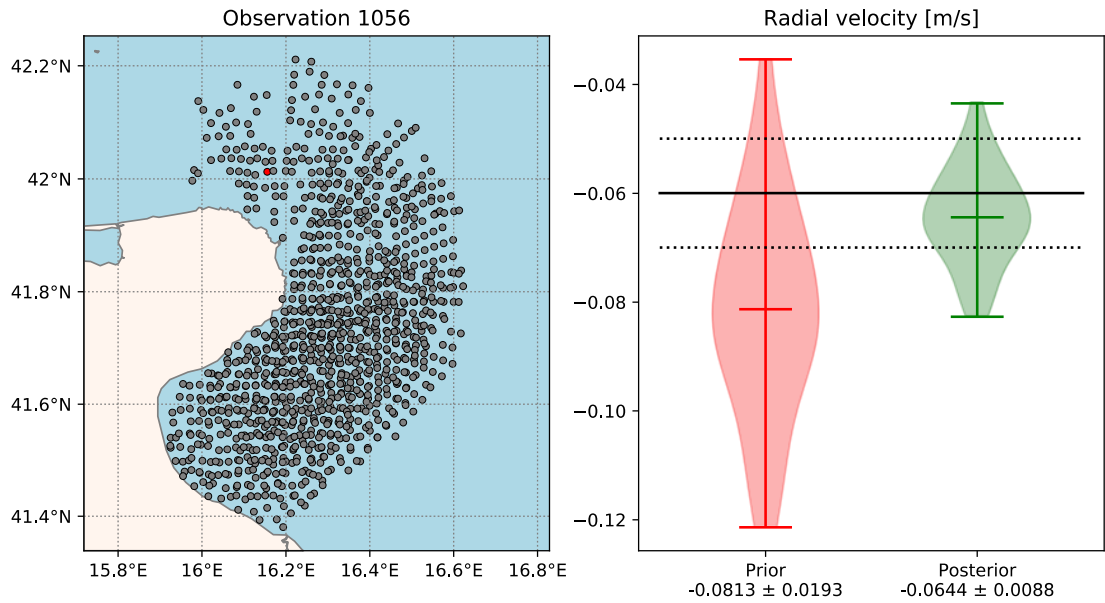


Figure 18: Result of assimilating a typical radial observation into the ensemble. On the left is a map of all observations in the assimilation window, with the current observation indicated in red. On the right is the value of the observation and its uncertainty indicated in black, with the prior ensemble in red and the posterior ensemble shown in green.

Figure 19 shows the results of the first two experiments in the form of a Taylor diagram. In this diagram the agreement between the model and the observations is expressed in terms of the amplitude of the variations (radial axis) and the correlation between the variations (angular axis). The reference indicates the observation itself, with perfect agreement being the same amplitude and a correlation equal to 1. The closer a model point lies to this reference, the better the performance of the model.

Each assimilation step consists of approximately 1000 observations, and each step is summarised in the figure by one point. This point indicates the agreement of the background observation prediction just prior to assimilating. The colour of the point indicates the sequence, from the first timestep (dark) to the last timestep (light). It can be seen that for $\sqrt{R} = 1$ cm/s the RMSE at all timesteps lies between 5 and 10 cm/s.

To test that this value for R is indeed optimal given the observations and the ensemble variability in the data assimilation setup, a second experiment was performed reducing the value of R to $\sqrt{R} = 0.5$ cm/s. The reduced observational errors means that the ensemble mean will be more strongly drawn towards the observed value and the ensemble spread will be further reduced. However, from Figure 19 it can be seen that this reduction does not result in better forecast capabilities for the ensemble. In fact the RMSE becomes 10-20% worse than with the larger uncertainty.

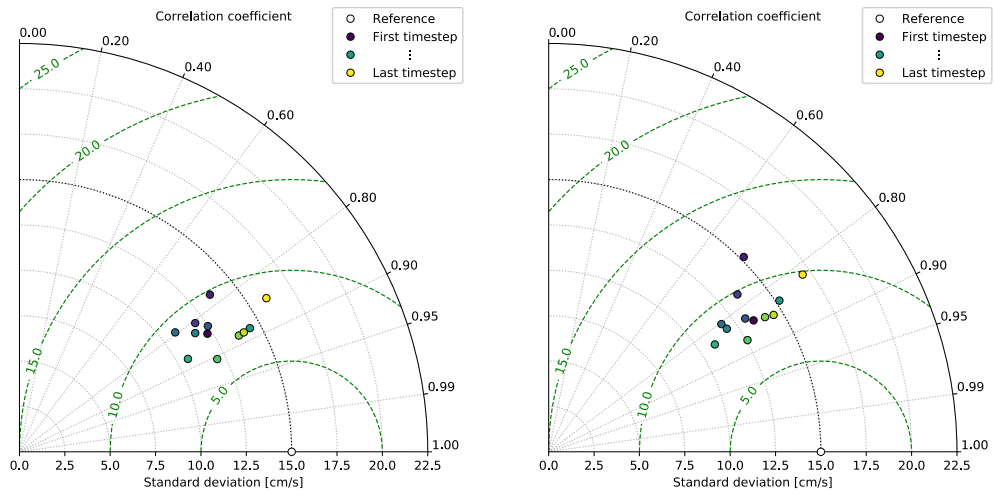


Figure 19: Taylor diagrams showing the result of daily assimilation of HF radar surface current velocities with $\sqrt{R} = 1$ cm/s (left) and $\sqrt{R} = 0.5$ cm/s (right).

Based on these results, a third experiment has been performed in which the assimilation frequency was increased from once per day to once per hour. The size of the assimilation window was kept as one hour, meaning that in this experiment all available HF radar observations (after thinning and gridding) are assimilated. The results of this experiment are shown in Figure 20. The hourly assimilation does not significantly improve the agreement of the model forecast and the radial observations. The RMSE are similar to those of experiment 1, with most timesteps resulting in an RMSE between 5 and 10 cm/s.

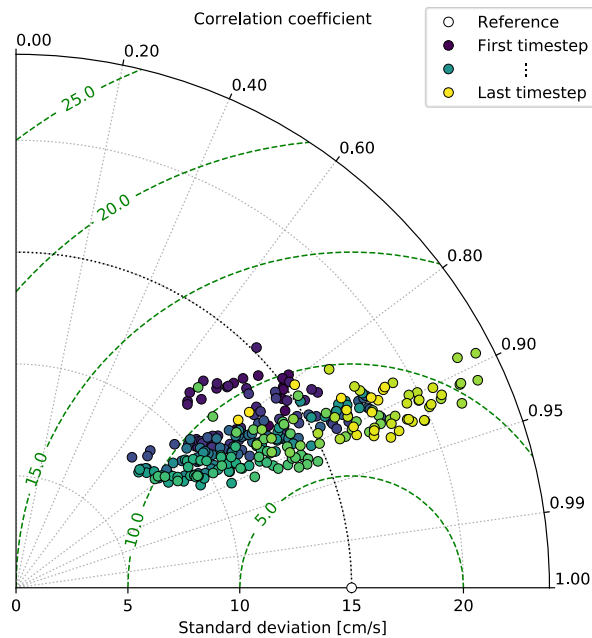


Figure 20: Taylor diagram showing the result of hourly assimilation of HF radar surface current velocities with $\sqrt{R} = 1$ cm/s.



Independent validation using surface drifters

In addition to validating the performance of the model with the observations being assimilated, the presence of surface drifters in the Gulf of Manfredonia during the time of these experiments allows a second, independent validation of the analysed state.

In order to compare the analysed model state to the drifter trajectories, the drifter trajectories are divided in sections that correspond to 6 hours of drift time. Each section is simulated individually, placing a virtual particle at the location of the drifter in the modelled velocity fields and advecting the particle using the 4th order Runge-Kutta scheme with a timestep of 30 minutes. The comparison is then made in terms of the average zonal and meridional speed of the particle/drifter in each of the 6-hour periods. Using the available drifters and the length of the assimilation period, this results in 208 observations that may be compared.

Figure 21 shows the results of this drifter validation in a Taylor diagram. First of all it should be noted that the performance is worse than when comparing to the HF radar observations. This can be readily understood, as the resolution of the AIFS model is 2.2km, which is rather coarse for modelling surface drifters on such a small scale. Nevertheless it offers a valid comparison of the various experiments and a useful validation of the HF radar assimilation capabilities of the system.

It can be shown from the figure that for all experiments the modelling of the u-component similarly well. This is most likely because the u-component most often coincides with the direction of measurement of the antennas and is therefore easiest to correct. In the experiments with daily assimilation (EXP1 and EXP2), the v-component improves very little compared to the AIFS model without assimilation. It might in fact become slightly worse. However, in the experiment with hourly assimilation (EXP3) it can be seen that the v-component does improve significantly. Compared to the drifter trajectories its agreement is now very similar to the u-component.

This is probably the result of the fact that the v-component is often close to perpendicular with the measurement direction of the radar antenna. As a result most observations contain only “partial” measurements of the v-component with a large uncertainty. The v-component therefore benefits most from the substantial increase in the number of observations cause by the hourly assimilation cycle.

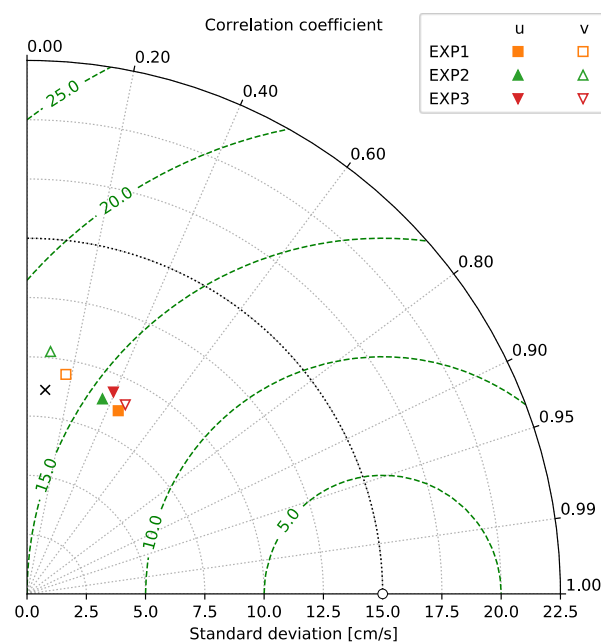


Figure 21: Taylor diagram of the drifter validation. The u - and v -components of each experiment are shown separately, indicated by closed (u) and open (v) markers. The colour and shape distinguish different experiments. The cross indicates the performance of the AIFS model without assimilating HF radar data and can be regarded as a baseline.

3.4.7. Evaluation of transport in NW Mediterranean Sea

In the Ligurian Sea, in the northwest Mediterranean, CNR-ISMAR operates a second HF radar network. This network is comprised of two antennas: located in Monterosso (MONT) and on Tino Island (TINO). Also data from this network has been assimilated into the AIFS-EnSRF DA system, with as its main goal to evaluate the impact of the assimilation on the modelling of transport in the area.

Two runs were performed from January to February 2017: a control run assimilating ARGO temperature and salinity profiles as usual; and an HFR run assimilating ARGO and the HFR data from the La Spezia system. As no actual drifter data was available in this period and area, the impact assessment is performed using the trajectories of virtual drifters. The drifters are released at regular distance within the radar coverage for both runs, allowing a comparison of their trajectories with and without HFR assimilation.

Figure 22 shows the results of the virtual drifter simulation for a one-week period. It can be seen that the HFR assimilation has a significant impact on the virtual drifters, making the smoothed out trajectories of the control run more realistic.

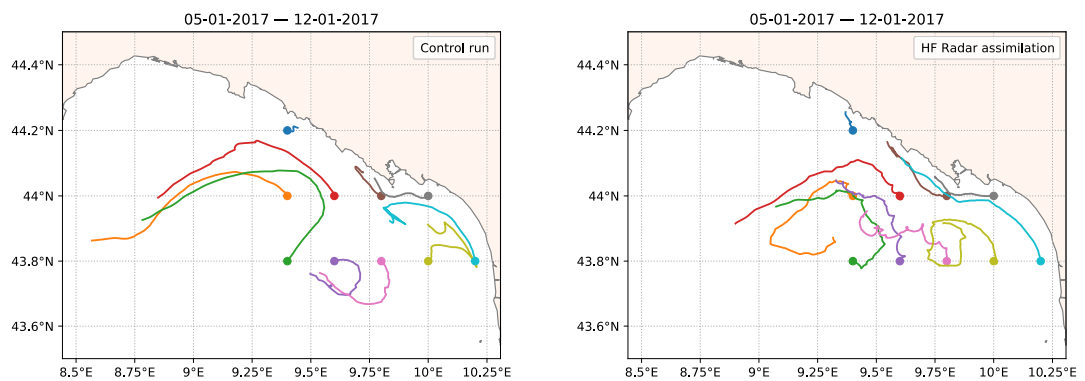


Figure 22: Virtual drifter trajectories modelled by the AIFS-EnSRF system without (left) and with HFR assimilation. The starting locations of the virtual drifters are indicated by the closed circles.



4. Outreach, dissemination and communication activities

N/A

5. Conclusions

The present deliverable described the main scientific approaches developed for the European Seas for defining the OSE/OSSE strategy in coastal zone. The results have been presented for the Bay of Biscay, the Ibiza Channel, the German Bight and the Central Mediterranean, with focus on the Adriatic Sea and the NW Mediterranean Sea. The approach will be used as backbone within WP4, in particular for JRAP4 and JRAP6.

6. Annexes and references

Bellafore, D. and Umgiesser, G. (2010). Hydrodynamic coastal processes in the north Adriatic investigated with a 3D finite element model, *Ocean Dynamics* 60 (2), 255-273, 2010.

Ciliberti, S. A., Pinardi, N., Coppini, G., Oddo, P., Vukicevic, T., Lecci, R., Verri, G., Kumkar, Y., Creti', S. (2015). A high resolution Adriatic-Ionian Sea circulation model for operational forecasting. *Geophysical Research Abstracts*, Vol.17, EGU2015-10899, 2015.

Engerdahl, H. (1995) Use of the flow relaxation scheme in a three-dimensional baroclinic ocean model with realistic topography. *Tellus*, 47A, 365–382.

Federico, I., Pinardi, N., Coppini, G., Oddo, P., Lecci, R., and Mossa, M.: Coastal ocean forecasting with an unstructured-grid model in the Southern Adriatic Northern Ionian Sea, *Nat. Hazards Earth Syst. Sci. Discuss.*, doi:10.5194/nhess-2016-169, in review, 2016.

Ferrarin, C., Roland, A., Bajo, M., Umgiesser, G., Cucco, A., Davolio, S., Buzzi, A., Malguzzi, P., and Drofa. O. (2013). Tide-surge-wave modelling and forecasting in the Mediterranean Sea with focus on the Italian coast, *Ocean Modelling*, 61, 38-48, 2013.

Flather, R. A. (1976). A tidal model of the northwest European continental shelf. *Mem. Soc. R. Sci. Liege, Ser. 6,10*, 141-164.

Halliwell Jr, GR, A Srinivasan, V Kourafalou, H Yang, D Willey, M Le Hénaff, and R Atlas. "Rigorous Evaluation of a Fraternal Twin Ocean OSSE System for the Open Gulf of Mexico." *Journal of Atmospheric and Oceanic Technology* 31, no. 1 (2014): 105–130.

Juza M., B. Mourre, L. Renault, S. Gómara, K. Sebastián, S. Lora, J.P. Beltran, B. Frontera, B. Garau, C. Troupin, M. Torner, E. Heslop, B. Casas, R. Escudier, G. Vizoso,, and J. Tintoré (2016). SOCIB operational ocean forecasting system and multi-platform validation in the western Mediterranean Sea, *J. Oper. Oceanogr.*, 9 :sup1, s155-s166, doi :10.1080/1755876X.2015.111

Madec, G. (2008). NEMO Ocean General Circulation Model Reference Manual, Internal Report, LODYC/IPSL, Paris, 2008.

Malacic, V., and Petelin, B. (2009). Climatic circulation in the Gulf of Trieste (northern Adriatic), *J. of Geophys. Res.*, 114: C07002.

Oddo, P., Adani, M., Pinardi, N., Fratianni, C., Tonani, and M., Pettenuzzo, D., (2009). A nested Atlantic-Mediterranean Sea general circulation model for operational forecasting. *Ocean Sci.*, 5: 461-473.





- Pacanowski, R.C. and Philander, S.G.H. (1981). Parametrization of vertical mixing in numerical models of tropical oceans, *J. Phys. Oceanogr.*, 11, 1443-1451, 1981.
- Pasaric, M. (2004). Annual cycle of river discharge along the Adriatic coast of Croatia. *Rapports et Proces-Verbaux des Reunions CIESMM* 37, 132.
- Pinardi, N., Allen, I., Demirov, E., De Mey, P., Korres, G., Lascaratos, A., Le Traon, P. Y., Maillard, C., Manzella, G., and Tziavos, C. (2003). The Mediterranean ocean forecasting system: first phase implementation (1998-2001). *Ann. Geophys.*, 2003, 21: 3-20.
- Raicich, F. (1996). Note on the flow rates of the Adriatic rivers. CNR, Istituto Talassografico di Trieste Tech. Rep. RF 02/94, 8 pp. Available from CNR-Istituto Talassografico di Trieste, viale Romolo Gessi 2, I-34123 Trieste, Italy.
- Schulz-Stellenfleth, J., and EV Stanev, "Combined assimilation of tide gauge water levels and HF radar surface currents in the German Bight based on the inversion of a two-layer barotropic model", in preparation, 2017
- Schulz-Stellenfleth, J, and EV Stanev. "Analysis of the Upscaling problem—A Case Study for the Barotropic Dynamics in the North Sea and the German Bight." *Ocean Modelling* 100 (2016): 109–124. doi:10.1016/j.ocemod.2016.02.002.
- Stanev, EV, F Ziemer, J Schulz-Stellenfleth, J Seemann, J Staneva, and K-W Gurgel. "Blending Surface Currents from HF Radar Observations and Numerical Modelling: Tidal Hindcasts and Forecasts." *Journal of Atmospheric and Oceanic Technology* 32 (2015): 256–81. doi:10.1175/JTECH-D-13-00164.1.
- Tonani, M., Pinardi, N., Dobricic, S., Pujol, I., and Fratianni, C. (2008). A high resolution free surface model of the Mediterranean Sea. *Ocean Sci. Discuss.*, 2008, 4: 213-244.
- Trotta, F., Fenu, E., Pinardi, N., Bruciaferri, D., Giacomelli, L., Federico, I., Coppini, G. (2016). A Structured and Unstructured grid Relocatable ocean platform for Forecasting (SURF). *Deep-Sea Research II*, in press.
- Umgiesser, G., Canu, D. M., Cucco, A., Solidoro, C. 2004. A finite element model for the Venice Lagoon. Development, set up, calibration and validation. *Journal of Marine Systems*, 51:1-4, pp.123-145.

